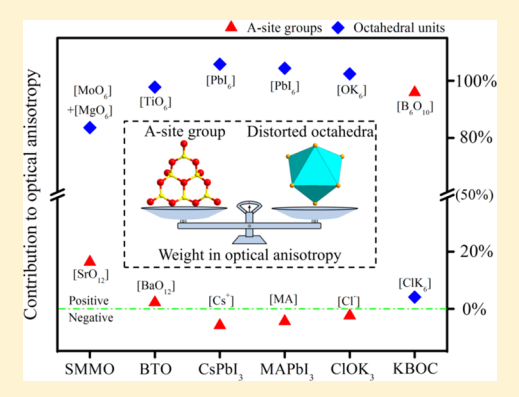
Cite This: J. Phys. Chem. C 2019. 123. 31167–31174

Transformation of Optical Anisotropy Origins in Perovskite-Related **Materials: A First-Principles Study**

Tinghao Tong, Ming-Hsien Lee, and Jun Zhang*, lo

Supporting Information

ABSTRACT: Perovskite-related compounds are of vital significance in the optical element and laser industry and other fields. Exploring the contributions of microscopic units that form the perovskite framework is one efficient way to design new materials with targeted performance. In this work, we acquired the linear and nonlinear optical properties and analyzed the superior functional units in determining optical anisotropy and second harmonic generation (SHG) of typical perovskite-related compounds from inorganic to organic, namely, BaTiO₃, Sr₂MgMoO₆, CsPbI₃, CH₃NH₃PbI₃, ClOK₃, and B₆O₁₀ClK₃. The results indicate that distorted octahedral units are dominant in optical anisotropy for the vast majority of perovskite-related compounds. For instance, [TiO₆], [Mo₆], [PbI₆], and [OK₆] octahedral units are decisive birefringence origins to BaTiO₃, Sr₂MgMoO₆, CsPbI₃ and CH₃NH₃PbI₃, and ClOK₃, respectively, most of which contribute over 90%. When it comes to B₆O₁₀ClK₂, it is A-site [B₆O₁₀] groups but not [ClK₆] octahedral units that lead the optical



anisotropy, as the A-site groups present stronger covalency than octahedral units. In addition, through SHG-density analysis, Asite $[B_6O_{10}]$ groups are also dominant SHG origins, which means A-site ionic groups are possible linear and nonlinear optical origins in this case.

1. INTRODUCTION

Downloaded via NATL TAIWAN UNIV on May 19, 2020 at 15:46:35 (UTC). See https://pubs.acs.org/sharingguidelines for options on how to legitimately share published articles.

In the field of linear and nonlinear optics, compounds are often sorted out by chemical composition or spatial structure because these two factors greatly influence optical properties. For instance, classified by chemical components, borates, ¹⁻⁷ phosphates, ⁸⁻¹¹ carbonates, ^{12,13} and so on have attracted much attention and been explored systematically. 14-19 In terms of spatial structure, materials with the frameworks akin to calcites, rutile, chalcopyrite, perovskite, and so forth are also outstanding optical categories that are worthy of attention. As is known to all, perovskite-related materials are superior not only in the solar cell but also in the optical element and other fields. 20-23 For example, hybrid inorganic-organic solar cell $(RNH_3)BX_3$ (where R is C_nH_{2n+1} , X is the halogen I, Br, or Cl, and B is Pb or Sn) with power conversion efficiency of over 10%, $^{24-26}$ optical anisotropy crystal BaTiS₃ with birefringence of 0.76, $^{27-29}$ nonlinear optical (NLO) material BaTiO₃ (BTO) with second harmonic generation (SHG) coefficient of 2.13 pm/V.³⁰ As structural distortion is closely related to optical properties, perovskite-related materials, which are susceptible to distortions, have won a place in NLO materials for their large tendency to reveal a noncentrosymmetric structure and large SHG response.⁶ For conventional perovskites, the octahedral unit is considered to be the main contributor to the SHG effect, according to the anionic group theory which is based on structural chemistry.³¹ In perovskite-related materials,

compared with conventional perovskites, A-site of the latter is likely occupied by ionic groups. For instance, K₃B₆O₁₀Cl (KBOC), ${}^{6}K_{3}B_{6}O_{10}Br$, ${}^{7,32}Na_{3}B_{6}O_{10}Br$, 33 and $Na_{3}B_{6}O_{10}Cl$, 3 which were reported by the Pan group. With the A-site ions replaced by ionic groups, the octahedral unit is not the unique ionic group that may impact optical properties.

As a prerequisite for optical materials, optical anisotropy is one of the most primary phenomena in optics, on which plenty of discoveries, inventions, and applications are based. Birefringent materials have attracted a great deal of academic and commercial interest, such as polarizer, wave plate, optical fiber isolator, phase-matching element, and so on. 35-38 In these aspects, calcite,³⁹ rutile,⁴⁰ yttrium vanadate,⁴¹ KTiOPO₄ (KTP),42 and the like are widely applied for their superior combination properties. In general, optical anisotropy is closely connected with covalent bonding behavior in terms of orientation. 43,44 Therefore, optical anisotropy is likely influenced by the covalent interaction of octahedral units as well as A-site ionic groups in perovskite-related compounds. There is no doubt that studying the bonding behavior and contributions of microscopic ionic groups is meaningful. Through rational analysis, contributory optical origins could

Received: September 5, 2019 Revised: November 8, 2019 Published: December 3, 2019

[†]School of Physical Science and Technology, Physical and Chemical Detecting Center, Xinjiang University, 666 Shengli Road, Urumqi 830046, China

^{*}Department of Physics, Tamkang University, New Taipei 25137, Taiwan

be distinguished and adopted to explore or design functional materials on purpose.45

In this work, to find the optical origins and explore superior functional units in determining optical anisotropy and SHG effect of the conventional perovskite and perovskite-related materials, BTO,⁵⁵ Sr₂MgMoO₆ (SMMO),⁵⁶ CsPbI₃,⁵⁷ CH₃NH₃PbI₃ (MAPbI₃),⁵⁸ ClOK₃,⁵⁹ and KBOC⁶ were systemically studied by multiple analysis methods. Generally speaking, birefringence is the difference between the maximum and minimum refractive indices in principal axes (the maximum value), and it could be obtained from dielectric functions. With regard to the relationship between optical anisotropy and bonding electron distribution, the response electron distribution anisotropy (REDA) approximation provides a rational settlement for covalent systems, which concerns the bonding electron density, bond valence, bond angle, and so forth. 47,60 Based on the REDA method, a larger REDA index reflects a larger contribution to the birefringence; therefore, the major contributor could be represented numerically. When it comes to compounds with weak covalence, the real-space atom-cutting (RSAC) method was adopted, which could analyze the properties of "changed crystal structure" by setting the band wave function as zero in the zones that belong to a specific ion or a cluster. 61 The results of the latter are consistent with the ones from the density functional theory (DFT)⁶² and REDA. Through rational analysis of multi-aspect, we found that octahedral units are the major contributors to optical anisotropy for most perovskite-related compounds. For instance, [TiO₆], [Mo₆], [PbI₆], and [OK₆] octahedral units are decisive origins to birefringence in BTO, SMMO, CsPbI₃ and MAPbI₃, and ClOK₃, respectively, most of which contribute more than 90%. However, in KBOC, A-site $[B_6O_{10}]$ groups acquire the leading role, as they present stronger covalent bonding behavior than octahedral units. A-site $[B_6O_{10}]$ groups are also main NLO origins by the SHG-density method. ⁶³ In general, octahedral units are the decisive optical origins for most perovskite-related materials. Although, when A-site ions are replaced by ionic groups with strong bonding behaviors like [B₆O₁₀], the origin of birefringence and SHG possibly transforms from the octahedral units to A-site groups.

2. CRYSTAL STRUCTURES

Crystallized in the P4mm space group, BTO consists of [TiO₆] octahedral units and A-site Ba²⁺ (Figure 1a). For the distorted $[TiO_6]$ octahedron (Figure S1a), observing in the c direction, four rotational symmetric Ti1-O2 bonds exhibit equal length, but two Ti1-O1 bonds along the c axis are in different extent—one is 1.8108 Å, whereas the other one is 2.2132 Å. In space group P1, SMMO possesses a general chemical formula of A2BB'X6, which is known as a double perovskite. Sharing common corners, [MgO₆] and [MoO₆] octahedral units are linked as a three-dimensional framework with Sr2+ located in the A-site (Figure 1b). In Figure S1b, γ-CsPbI₃ is crystallized in a centrosymmetry space group Pnam, and Cs+ is surrounded by slant [PbI₆] octahedra. As shown in Figure 1c, MAPbI₃ is made up of [CH3NH3] groups and the three-dimensional framework composed of [PbI₆] octahedra. Especially, it could be seen as a substitution of Cs⁺ by [CH₃NH₃] in CsPbI₃, as their octahedral frameworks are quite similar to each other.⁶⁴ In Figure S1c, ClOK₃ is made up of [OK₆] octahedral units and A-site Cl⁻. KBOC crystallizes in the trigonal crystal system with the space group of R3m (Figure 1d). Comparing KBOC

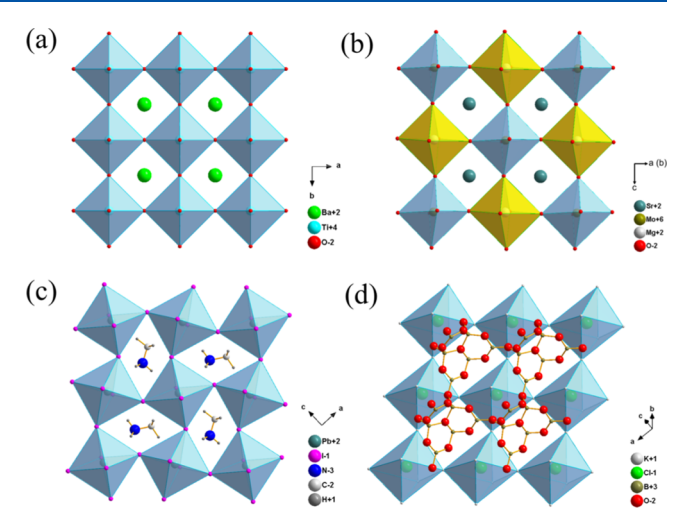


Figure 1. Crystal structures of BTO (a), SMMO (b), MAPbI₂ (c) and KBOC (d).

with conventional perovskite CaTiO₃, A-site [B₆O₁₀] ionic groups that consist of [BO₃] and [BO₄] units occupy the positions of atom Ca, whereas atom Cl takes up the positions of atom Ti, and the positions of atom K are similar to those of O. Therefore, analogous to conventional perovskite CaTiO₃, KBOC could be represented as the formula of (B₆O₁₀)ClK₃. Details of the crystal symmetry and unit cell dimensions for these compounds are listed in Table 1.

Table 1. Crystal Symmetry and Unit Cell Dimensions of Compounds Analyzed in This Work

compound	space	group	symmetry	unit cell dimensions (Å)
ВТО	P4mm	no. 99	NCS	4.0000(2), 4.0000(2), 4.0240(2)
SMMO	$P\overline{1}$	no. 2	CS	5.56906(4), 5.57039(4), 7.92407(5)
$MAPbI_3$	Pnma	no. 62	CS	8.86574(30), 12.6293(4), 8.57689(31)
$CsPbI_3$	Pnam	no. 62	CS	8.8561(4), 8.5766(3), 12.4722(6)
ClOK ₃	Pbnm	no. 62	CS	7.239(2), 7.239(2), 10.277(2)
B ₆ O ₁₀ ClK ₃	R3m	no. 160	NCS	10.0624(14), 10.0624(14), 8.8361(18)

3. CALCULATION DETAILS

The electronic structures were obtained by ab initio calculations implemented in the CASTEP package.⁶⁵ The calculations of all crystals were done on experimental structures, and the generalized gradient approximation (GGA) with the Perdew-Burke-Ernzerhof functional⁶⁶ was employed for the exchange-correlation potential. The planewave basis set energy cutoff was 900 eV with Norm-conserving pseudopotential, and the Monkhorst-Pack⁶⁷ scheme was given by $6 \times 6 \times 6$, $6 \times 6 \times 4$, $6 \times 6 \times 4$, $6 \times 4 \times 6$, $6 \times 6 \times 4 \times 6$ 6×4 , $6 \times 6 \times 6$ for BTO, SMMO, CsPbI₃, MAPbI₃, ClOK₃, and KBOC in the irreducible Brillouin zone. To ensure the convergence of optical properties, the empty bands were set as three times the number of valence bands in this work. Because of the strong relativistic effect of Pb, spin-orbit coupling (SOC) was previously reported for CsPbI₃ and MAPbI₃. However, the errors of GGA and SOC could counteract with

each other to some degree. ²⁶ Therefore, the GGA provides more close results to experiment than GGA + SOC, and thus the GGA without SOC was adopted in this work. Adopting the parameters described above, calculation results of the birefringence for several known optical crystals such as calcite, rutile, YVO₄, and KTP are tabulated in Table 2. The results basically agree with experimental values, indicating the validity of the method used in this work.

Table 2. Calculated and Experimental Birefringence of Some Known Optical Materials under the Same Calculation Conditions in This Work

compound	space group	wavelength (nm)	Δn (cal.)	Δn (exp.)
CaCO ₃	$R\overline{3}c$	@533	0.161	0.174^{39}
TiO_2	$P4_2/mnm$	@1500	0.231	0.249^{40}
YVO_4	$I4_1/amd$	@1550	0.208	0.206^{41}
KTP	$Pna2_1$	@1064	0.089	0.085^{42}

Under REDA approximation, the birefringence can be estimated by the anisotropic valence bond of anionic groups as

$$\Delta n = \frac{\mathcal{R} \sum_{g} \left[N_{c} Z_{a} \Delta \rho^{b} \right]_{g}}{2n_{l} E_{o}} \tag{1}$$

Here, \mathcal{R} is the correction coefficient, $N_{\rm c}$ is the coordination number of the nearest neighbor cations to the central anion, $Z_{\rm a}$ is the formal chemical valence of the anion, $\Delta \rho^{\rm b}$ is the difference between the maximum and minimum bonding electron density of covalent bond in an anionic group on the optical principal axes of a crystal, $E_{\rm o}$ is the optical band gap, $n_{\rm 1}$ is the minimum refractive index and usually has little change in a system. In this formula, $\zeta = \sum_{g} [N_{\rm c} Z_{\rm a} \Delta \rho^{\rm b}/(n_{\rm 1} E_{\rm o})]_g$ is called

the REDA index, which could be employed to characterize the optical anisotropy of materials. ^{47,60} In the process of REDA calculation for BTO, SMMO, and KBOC, A-site ionic groups and octahedral units were analyzed separately. To further confirm the conclusions as well as to make a supplement for CsPbI₃ and MAPbI₃ which present weak covalence, the RSAC method was adopted. In detail, Cs⁺, [MA], Cl⁻, and [KCl₆] were "cut" from CsPbI₃, MAPbI₃, ClOK₃, and KBOC, respectively, to measure and compare the contributions of the A-site groups and octahedral units. The units were cut according to the ionic radius with corresponding charge (Table S1).

4. RESULTS AND DISCUSSION

4.1. Electronic Structures. Band structures and the partial density of states (PDOS) of the title compounds were calculated along the high symmetry lines. As shown in Figure 2a, BTO exhibits a 1.94 eV indirect optical band gap, which is smaller than the experimental value 3.27 eV due to the discontinuity of the derivative on exchange—correlation energy within DFT. An energy shift in the conduction bands or a so-called scissors operator was introduced to calculate optical properties in order to overcome such a difference, ⁶⁸ and the value is 1.33 eV in this case. KBOC shows a direct band gap of 5.31 eV (Figure 2b). Compared with the experimental result of 6.89 eV, the scissors operator of 1.58 eV was adopted. Calculated and experimental band gaps of the other four compounds are listed in Table 3.

The composition and origin of calculated bands could be obtained by analyzing the PDOS. In Figure 2a, the main states that determine the gap and electronic transitions are in the range of -5 to 10 eV near the Fermi surface for BTO. The top of the valence bands is greatly composed of O-p orbitals,

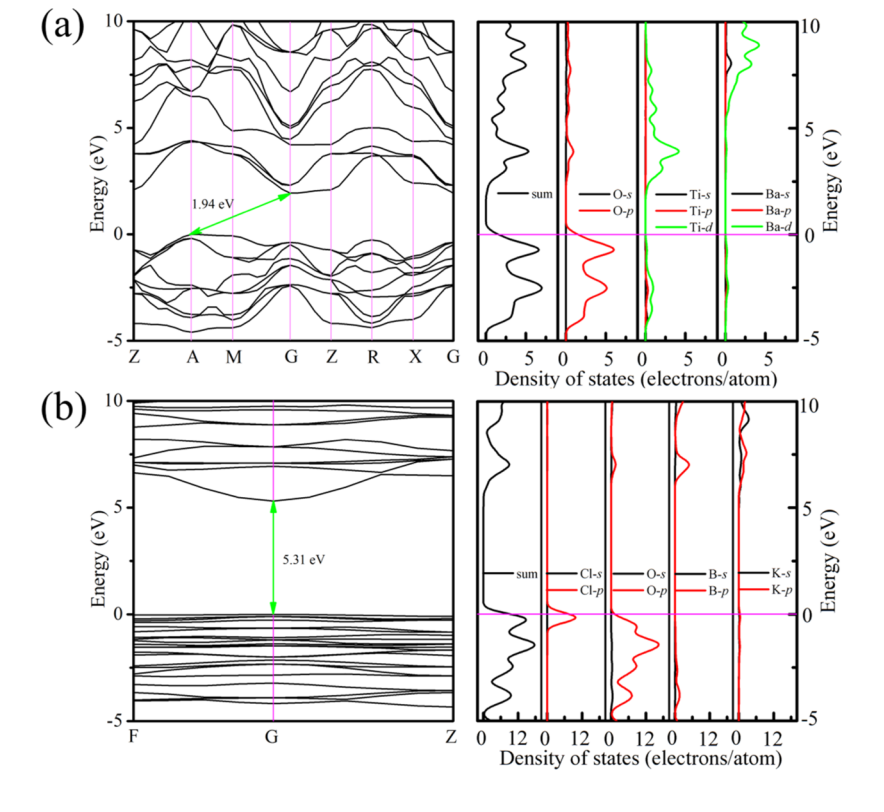


Figure 2. Band structures and PDOS of BTO (a) and KBOC (b).

Table 3. Calculated and Experimental Band Gaps, SHG Coefficients (d_{ij}) , and Birefringence (Δn) with the Corresponding Wavelength of the Title Compounds

compound	band gap (eV) (cal./exp.)	d _{ij} (pm/V) (cal./exp.)	Δn (cal./exp.)	wavelength (nm)			
ВТО	$1.94/3.27^{69}$	$2.09/2.13^{30}$	$0.059/0.051^{70}$	@633			
SMMO	1.90/3.16 ^a		0.016/—	@1064			
$CsPbI_3$	$2.08/2.13^a$		0.275/—	@1064			
$MAPbI_3$	$2.07/2.13^a$		0.292/—	@1064			
$ClOK_3$	$0.91/2.35^a$		0.042/—	@1064			
KBOC	5.31/6.89 ⁶	$1.02/1.56^6$	$0.046/0.046^{71}$	@1064			
^a Obtained by PWmat code ⁷² HSE06.							

whereas the bottom of the conduction bands is mainly derived from Ti-d orbitals and marginally from O-p orbitals. For KBOC (Figure 2b), the top of the valence bands is greatly composed of Cl-p and O-p orbitals, and the bottom of the conduction bands is mainly derived from B-p orbitals. As is well-known, electron transition near the Fermi surface determines material optical properties. Therefore, it is likely that $[TiO_6]$ octahedron is the decisive optical origin for BTO, whereas the B–O group makes more contributions than $[KCl_6]$ octahedral units to optical properties in KBOC. Band structures and PDOS of the other four compounds are presented in Figure S2. Similar to the analysis above, $[MoO_6]$, $[PbI_6]$, and $[OK_6]$ octahedral units are likely dominant in optical properties for SMMO, CsPbI₃, MAPbI₃, and ClOK₃ crystals.

4.2. Linear and NLO Properties. Described by birefringence (Δn) , optical anisotropy could be obtained in the form of dispersion refractive indices. Calculated and experimental birefringence are shown in Table 3. BTO exhibits moderate optical anisotropy of 0.059 at 633 nm, and the birefringence of KBOC is 0.046 at 1064 nm. Comparatively, SMMO shows a smaller birefringence of 0.016. With similar [PbI₆] octahedral frameworks, CsPbI₃ and MAPbI₃ exhibit the large optical anisotropy of 0.275 and 0.292 at 1064 nm. In addition, theoretical calculations of SHG coefficients were also performed, and the results are listed in Table 3 as well. Crystallized in centrosymmetry space groups, SMMO, CsPbI₃, and MAPbI3 conduct no SHG response. For BTO and KBOC, the SHG coefficients are $d_{15} = 2.13 \text{ pm/V}$ and $d_{22} = 1.56 \text{ pm/}$ V, respectively, which are much larger than that of potassium dihydrogen phosphate ($d_{36} = 0.39 \text{ pm/V}$) and enough for ultraviolet (UV)/ deep UV (DUV) light frequency conversion.

4.3. Origins of Optical Properties. The total electron density (TED) clearly reflects the redistribution of electrons by the form of density maps. In order to make the electron

distribution distinguishable and comparable, a uniform density criterion was adopted for BTO and KBOC (Figure 3). In BTO, observing from the *b* axis, the electron density around Ti1 overlaps with O2 along the Ti1–O2 direction (Figure 3a). At the same time, more conspicuous electron density overlaps show up between Ti1 and O1, which are closely associated with distorted [TiO₆] octahedra described in the crystal structure paragraph. It is worth noting that, in Figure 3b, the spherical appearances of electron density are uniform and isolated around Ba1 atoms. Therefore, the Ti–O bond tends to present more stronger covalency than the Ba–O bond. Taking the relationship between optical properties and covalent behavior into consideration, this phenomenon illustrates that the contributions of [TiO₆] octahedra are likely to exceed that of Ba–O units.

When it comes to KBOC shown in Figure 4a, under the same density criterion with BTO, there is no overlap between Cl^- and K^+ . Meanwhile, the electron density of $[B_6O_{10}]$, which consists of [BO₄] (Figure 4a,b) and [BO₃] (Figure 4c) units, shows great overlap along B-O bonds, and no barrier appears within the group. In other words, the [B₆O₁₀] groups exhibit more powerful covalency than the [ClK₆] octahedral units, tending to lead the optical anisotropy in KBOC. TED maps with a lower density criterion (Figure S3a) of the other four compounds are shown in Figure S3. For SMMO, there are strong overlaps along the Mo-O bonds, whereas Mg-O shows weak overlaps comparatively which are slightly stronger than the Sr-O bonds. Compared with SMMO, there are few overlaps in CsPbI₃, MAPbI₃, and ClOK₃ along the Pb-I and O-K bonds, whereas no overlaps are present among the A-site groups. In general, octahedral units exhibit stronger bonding behavior than A-site groups in most title compounds, tending to lead the optical anisotropy and NLO properties.

Especially, REDA and RSAC methods were adopted for further optical anisotropy analysis. By REDA approximation, the $\Delta \rho$ of the A-site ionic groups and octahedral units on the optical principal axes were analyzed, respectively. As shown in Figure 5, for SMMO, where the quantity ratio of $[MgO_6]$ and [MoO₆] octahedra is 1:1, Mg-O bonds exhibit weak covalence which is close to that of Sr-O bonds (Figure S3a). As a result, A-site [SrO₁₂] units make about 20% contributions to birefringence. In BTO, $\Delta \rho$ of the [TiO₆] and the [BaO₁₂] units are 0.002585 and 0.000058, respectively, which indicates that the [TiO₆] units make about 97.8% of the source of birefringence. However, when it comes to KBOC, $\Delta \rho$ of the [ClK₆] units and the [B₆O₁₀] groups are 0.000482 and 0.011414, respectively, making about 4.1 and 95.9% contributions to optical anisotropy. To further verify the consequence from REDA and make a supplement for

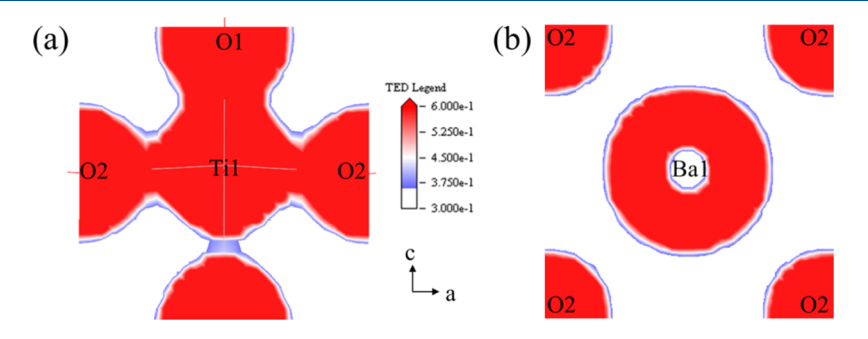


Figure 3. TED of $[TiO_6]$ unit (a) and $[BaO_{12}]$ group (b) in BTO along the b axis.

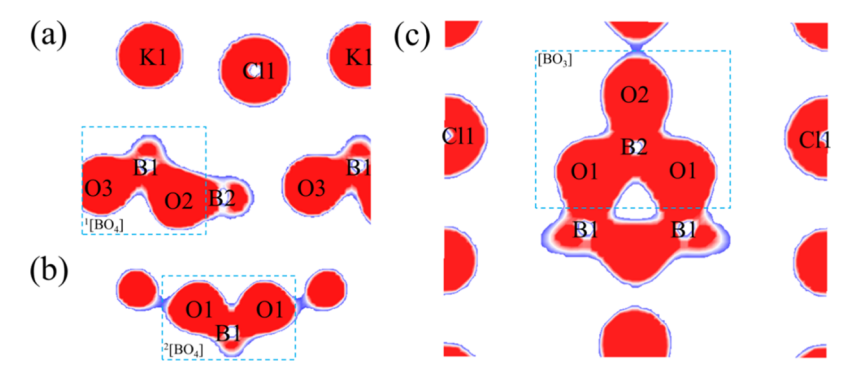


Figure 4. TED of $[ClK_6]$ unit (a) and $[B_6O_{10}]$ group, which consist of $[BO_4]$ [a combination of $^1[BO_4]$ (a) and $^2[BO_4]$ (b)] and $[BO_3]$ (c), and the direction is shown in Figure S4.

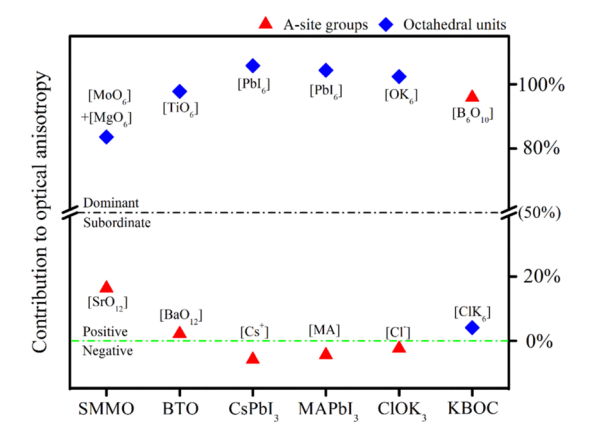


Figure 5. Group contributions of title compounds to optical anisotropy by REDA and RSAC.

compounds with weak covalency, the RSAC method was introduced. In CsPbI₃, the [PbI₆] framework presents a birefringence of 0.291, which is larger than the value 0.275 of the entirety. Therefore, [PbI₆] octahedra contribute 105.8%, whereas Cs⁺ contribute about -5.8%. In MAPbI₃, without [MA] units, the left [PbI₆] octahedra exhibit a birefringence of about 0.305. Compared with the result of 0.292, about 104.5% of influence is exerted by [PbI₆] octahedra. For ClOK₃, [OK₆] units contribute 102.4%, and Cl⁻ take about -2.4%. However, in KBOC, the left [B₆O₁₀] units make about 97.8% contributions (the ratio of 0.045-0.046), and it is in good accordance with the result of 95.9% from REDA. Details of the REDA and RSAC results of title compounds are listed in Table S2.

The SHG-density method, which could visualize the SHG response from electronic states, was adopted to analyze the contributions of various ionic groups. As shown in Figure 6a, the SHG density of occupied and unoccupied states indicates that there is almost no contribution to the SHG response from the Ba–O units. In contrast, $[\text{TiO}_6]$ octahedra exhibit a strong SHG response. When it comes to KBOC, the contributions of $[\text{CIK}_6]$ octahedra are appreciable and not negligible. As shown in Figure 6b, comparatively speaking, the A-site B–O units provide more powerful contributions than those from the distorted $[\text{CIK}_6]$ octahedra, as the unoccupied state of O^{2-} is more distinct than that of CI^- .

5. CONCLUSIONS

In conclusion, we have successfully acquired the optical properties and explored the contributions of microscopic groups to optical anisotropy and NLO response on crystal structure and bond character in conventional perovskite and perovskite-related materials. For BTO, SMMO, CsPbI₃, MAPbI₃, and ClOK₃ crystals, [TiO₆], [MoO₆], [PbI₆], and [OK₆] octahedral units are the major origins to birefringence, most of which make over 90% contributions. But in KBOC, the A-site [B₆O₁₀] groups contribute over an order of magnitude more than the [ClK₆] octahedron. Moreover, by the SHG-density analysis, the [B₆O₁₀] group is also the dominant NLO origin in KBOC. In general, octahedral units are the major contributors to both linear and NLO properties in most perovskite-related compounds. However, in KBOC, where the A-site ionic groups present stronger bonding behavior than octahedral units, the A-site ionic group still possibly performs as the main optical origin. We believe this

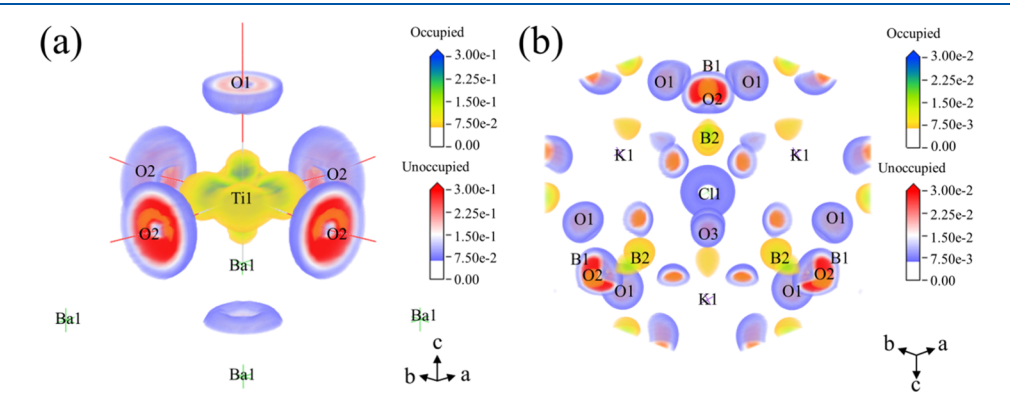


Figure 6. SHG density of occupied and unoccupied states in BTO and KBOC.

work will be helpful to gain more awareness about perovskiterelated compounds in microscopic structure, electron distribution, as well as optical properties, or provide inspiration to explore materials with targeted performance.

ASSOCIATED CONTENT

S Supporting Information

The Supporting Information is available free of charge at https://pubs.acs.org/doi/10.1021/acs.jpcc.9b08478.

Distorted [TiO₆] octahedral units in BTO and structures of CsPbI₃ and ClOK₃; band structures and PDOS of SMMO, CsPbI₃, MAPbI₃, and ClOK₃; TED of SMMO, CsPbI₃, MAPbI₃ and ClOK₃; TED planes of [BO₃], 1 [BO₄], and 2 [BO₄] in KBOC lattice; cut ionic radius for MAPbI₃, ClOK₃, and KBOC in RSAC method; and REDA contribution ($\Delta \rho$) of measured units and RSAC results (Δn) of left units after atom-cutting. (PDF)

AUTHOR INFORMATION

Corresponding Author

*E-mail: zhangjunxju@163.com.

ORCID

Jun Zhang: 0000-0001-8143-0042

Notes

The authors declare no competing financial interest.

ACKNOWLEDGMENTS

This work is supported by the National Natural Science Foundation of China (grant no. 11564038). M.-H.L. is grateful for the database service provided by NCHC (Taiwan) and computer equipment donated by KeyWin Inc.

■ REFERENCES

- (1) Mutailipu, M.; Zhang, M.; Yang, Z.; Pan, S. Targeting the Next Generation of Deep-Ultraviolet Nonlinear Optical Materials: Expanding from Borates to Borate Fluorides to Fluorooxoborates. *Acc. Chem. Res.* **2019**, *52*, 791–801.
- (2) Tran, T. T.; Yu, H.; Rondinelli, J. M.; Poeppelmeier, K. R.; Halasyamani, P. S. Deep Ultraviolet Nonlinear Optical Materials. *Chem. Mater.* **2016**, 28, 5238–5258.
- (3) Halasyamani, P. S.; Zhang, W. Viewpoint: Inorganic Materials for UV and Deep-UV Nonlinear-Optical Applications. *Inorg. Chem.* **2017**, *56*, 12077–12085.
- (4) Shi, G.; Wang, Y.; Zhang, F.; Zhang, B.; Yang, Z.; Hou, X.; Pan, S.; Poeppelmeier, K. R. Finding the Next Deep-Ultraviolet Nonlinear Optical Material: NH₄B₄O₆F. *J. Am. Chem. Soc.* **2017**, *139*, 10645–10648
- (5) Wang, X.; Wang, Y.; Zhang, B.; Zhang, F.; Yang, Z.; Pan, S. CsB₄O₆F: A Congruent-Melting Deep-Ultraviolet Nonlinear Optical Material by Combining Superior Functional Units. *Angew. Chem., Int. Ed. Engl.* **2017**, *56*, 14119–14123.
- (6) Wu, H.; Pan, S.; Poeppelmeier, K. R.; Li, H.; Jia, D.; Chen, Z.; Fan, X.; Yang, Y.; Rondinelli, J. M.; Luo, H. K₃B₆O₁₀Cl: a new structure analogous to perovskite with a large second harmonic generation response and deep UV absorption edge. *J. Am. Chem. Soc.* **2011**, *133*, 7786–7790.
- (7) Zhang, M.; Pan, S.-L.; Fan, X.-Y.; Zhou, Z.-X.; Poeppelmeier, K. R.; Yang, Y. Crystal growth and optical properties of a non-centrosymmetric haloid borate, K₃B₆O₁₀Br. *CrystEngComm* **2011**, *13*, 2899.
- (8) Chen, J.; Xiong, L.; Chen, L.; Wu, L.-M. Ba₂NaClP₂O₇: Unprecedented Phase Matchability Induced by Symmetry Breaking

- and Its Unique Fresnoite-Type Structure. J. Am. Chem. Soc. 2018, 140, 14082–14086.
- (9) Li, Z.; Liu, Q.; Han, S.; Iitaka, T.; Su, H.; Tohyama, T.; Jiang, H.; Dong, Y.; Yang, B.; Zhang, F.; Yang, Z.; Pan, S. Nonlinear electronic polarization and optical response in borophosphate BPO₄. *Phys. Rev. B* **2016**, 93, 245125.
- (10) Li, Z.; Liu, Q.; Wang, Y.; Iitaka, T.; Su, H. B.; Tohyama, T.; Yang, Z. H.; Pan, S. L. Second-harmonic generation in non-centrosymmetric phosphates. *Phys. Rev. B* **2017**, *96*, 035205.
- (11) Yu, P.; Wu, L.-M.; Zhou, L.-J.; Chen, L. Deep-ultraviolet nonlinear optical crystals: $Ba_3P_3O_{10}X$ (X = Cl, Br). J. Am. Chem. Soc. **2014**, 136, 480–487.
- (12) Luo, M.; Song, Y.; Lin, C.; Ye, N.; Cheng, W.; Long, X. Molecular Engineering as an Approach To Design a New Beryllium-Free Fluoride Carbonate as a Deep-Ultraviolet Nonlinear Optical Material. *Chem. Mater.* **2016**, *28*, 2301–2307.
- (13) Luo, M.; Wang, G.; Lin, C.; Ye, N.; Zhou, Y.; Cheng, W. $Na_4La_2(CO_3)_5$ and $CsNa_5Ca_5(CO_3)_8$: two new carbonates as UV nonlinear optical materials. *Inorg. Chem.* **2014**, *53*, 8098–8104.
- (14) Kang, L.; Liang, F.; Lin, Z.; Liu, F.; Huang, B. Cyano-Based Materials with Giant Optical Anisotropy and Second Harmonic-Generation Effect. *Inorg. Chem.* **2018**, *57*, 15001–15008.
- (15) Chen, M.-C.; Wu, L.-M.; Lin, H.; Zhou, L.-J.; Chen, L. Disconnection enhances the second harmonic generation response: synthesis and characterization of Ba₂₃Ga₈Sb₂S₃₈. *J. Am. Chem. Soc.* **2012**, *134*, 6058–6060.
- (16) Kim, Y. H.; Tran, T. T.; Halasyamani, P. S.; Ok, K. M. Macroscopic polarity control with alkali metal cation size and coordination environment in a series of tin iodates. *Inorg. Chem. Front.* **2015**, *2*, 361–368.
- (17) Liang, M.-L.; Hu, C.-L.; Kong, F.; Mao, J.-G. BiFSeO₃: An Excellent SHG Material Designed by Aliovalent Substitution. *J. Am. Chem. Soc.* **2016**, *138*, 9433–9436.
- (18) Sun, C.-F.; Hu, C.-L.; Xu, X.; Yang, B.-P.; Mao, J.-G. Explorations of new second-order nonlinear optical materials in the potassium vanadyl iodate system. *J. Am. Chem. Soc.* **2011**, *133*, 5561–5572.
- (19) Zhou, H.-M.; Xiong, L.; Chen, L.; Wu, L.-M. Dislocations that Decrease Size Mismatch within the Lattice Leading to Ultrawide Band Gap, Large Second-Order Susceptibility, and High Nonlinear Optical Performance of AgGaS₂. Angew. Chem., Int. Ed. Engl. **2019**, 58, 9979–9983
- (20) Liao, W. Q.; Zhang, Y.; Hu, C. L.; Mao, J. G.; Ye, H. Y.; Li, P. F.; Huang, S. D.; Xiong, R. G. A lead-halide perovskite molecular ferroelectric semiconductor. *Nat. Commun.* **2015**, *6*, 7338.
- (21) Lee, M. M.; Teuscher, J.; Miyasaka, T.; Murakami, T. N.; Snaith, H. J. Efficient hybrid solar cells based on meso-superstructured organometal halide perovskites. *Science* **2012**, *338*, 643–647.
- (22) Im, J.-H.; Lee, C.-R.; Lee, J.-W.; Park, S.-W.; Park, N.-G. 6.5% efficient perovskite quantum-dot-sensitized solar cell. *Nanoscale* **2011**, 3, 4088–4093.
- (23) Kim, H.-S.; Lee, C.-R.; Im, J.-H.; Lee, K.-B.; Moehl, T.; Marchioro, A.; Moon, S. J.; Humphry-Baker, R.; Yum, J.-H.; Moser, J. E.; Grätzel, M.; Park, N.-G. Lead iodide perovskite sensitized all-solid-state submicron thin film mesoscopic solar cell with efficiency exceeding 9%. Sci. Rep. 2012, 2, 591.
- (24) Cheng, Z.; Lin, J. Layered organic—inorganic hybrid perovskites: structure, optical properties, film preparation, patterning and templating engineering. *CrystEngComm* **2010**, *12*, 2646.
- (25) Liu, M.; Johnston, M. B.; Snaith, H. J. Efficient planar heterojunction perovskite solar cells by vapour deposition. *Nature* **2013**, *501*, 395–398.
- (26) Mosconi, E.; Amat, A.; Nazeeruddin, M. K.; Grätzel, M.; De Angelis, F. First-Principles Modeling of Mixed Halide Organometal Perovskites for Photovoltaic Applications. *J. Phys. Chem. C* **2013**, *117*, 13902–13913.
- (27) Hahn, H.; Mutschke, U. Untersuchungen ber ternre Chalkogenide. XI. Versuche zur Darstellung von Thioperowskiten. Z. Anorg. Allg. Chem. 1957, 288, 269–278.

- (28) Huster, J. Notizen: Die Kristallstruktur von BaTiS₃/Crystal Structure of BaTiS₃. Z. Naturforsch., B **1980**, 35, 775.
- (29) Niu, S.; Joe, G.; Zhao, H.; Zhou, Y.; Orvis, T.; Huyan, H.; Salman, J.; Mahalingam, K.; Urwin, B.; Wu, J.; Liu, Y.; Tiwald, T. E.; Cronin, S. B.; Howe, B. M.; Mecklenburg, M.; Haiges, R.; Singh, D. J.; Wang, H.; Kats, M. A.; Ravichandran, J. Giant optical anisotropy in a quasi-one-dimensional crystal. *Nat. Photonics* **2018**, *12*, 392–396.
- (30) Bihari, B.; Kumar, J.; Stauf, G. T.; Van Buskirk, P. C.; Hwang, C. S. Investigation of barium titanate thin films on MgO substrates by second-harmonic generation. *J. Appl. Phys.* **1994**, *76*, 1169–1174.
- (31) Chen, C.; Wu, Y.; Li, R. The anionic group theory of the nonlinear optical effect and its applications in the development of new high-quality NLO crystals in the borate series. *Int. Rev. Phys. Chem.* **2008**. *8*, 65–91.
- (32) Zhang, M.; Su, X.; Pan, S.; Wang, Z.; Zhang, H.; Yang, Z.; Zhang, B.; Dong, L.; Wang, Y.; Zhang, F.; Yang, Y. Linear and Nonlinear Optical Properties of K₃B₆O₁₀Br Single Crystal: Experiment and Calculation. *J. Phys. Chem. C* **2014**, *118*, 11849–11856.
- (33) Chen, Z.; Pan, S.; Dong, X.; Yang, Z.; Zhang, M.; Su, X. Exploration of a new compound in the M–B–O–X (M: alkali metals; X: halogen) system: Preparation, crystal and electronic structures, and optical properties of Na₃B₆O₁₀Br. *Inorg. Chim. Acta* **2013**, *406*, 205–210.
- (34) Bai, C.; Yu, H.; Han, S.; Pan, S.; Zhang, B.; Wang, Y.; Wu, H.; Yang, Z. Effect of halogen (Cl, Br) on the symmetry of flexible perovskite-related framework. *Inorg. Chem.* **2014**, 53, 11213–11220.
- (35) Nicholls, L. H.; Rodríguez-Fortuño, F. J.; Nasir, M. E.; Córdova-Castro, R. M.; Olivier, N.; Wurtz, G. A.; Zayats, A. V. Ultrafast synthesis and switching of light polarization in nonlinear anisotropic metamaterials. *Nat. Photonics* **2017**, *11*, 628–633.
- (36) Oka, K.; Kaneko, T. Compact complete imaging polarimeter using birefringent wedge prisms. *Opt. Express* **2003**, *11*, 1510–1519.
- (37) Weber, M. F.; Stover, C. A.; Gilbert, L. R.; Nevitt, T. J.; Ouderkirk, A. J. Giant birefringent optics in multilayer polymer mirrors. *Science* **2000**, 287, 2451–2456.
- (38) Zhang, W.; Yu, H.; Wu, H.; Halasyamani, P. S. Phase-Matching in Nonlinear Optical Compounds: A Materials Perspective. *Chem. Mater.* **2017**, *29*, 2655–2668.
- (39) Ghosh, G. Dispersion-equation coefficients for the refractive index and birefringence of calcite and quartz crystals. *Opt. Commun.* **1999**, *163*, 95–102.
- (40) Sinton, W. M. Birefringence of Rutile in the Infrared. J. Opt. Soc. Am. 1961, 51, 1309 1.
- (41) Goldstein, D. H.; DeShazer, L. G.; Chenault, D. B.; Egan, W. G.; Duggin, M. J. Improved midinfrared polarizers using yttrium vanadate. *Proc. SPIE* **2002**, *4481*, 10.
- (42) Bierlein, J. D.; Vanherzeele, H. Potassium titanyl phosphate: properties and new applications. *J. Opt. Soc. Am. B* **1989**, *6*, 622.
- (43) Wang, X.; Xia, M.; Li, R. K. A promising birefringent crystal Ba₂Na₃(B₃O₆)₂F. Opt. Mater. **2014**, 38, 6–9.
- (44) Li, R. On the calculation of refractive indices of borate crystals based on group approximation. *Z. Kristallogr.—Cryst. Mater.* **2013**, 228, 526–531.
- (45) Dyer, M. S.; Collins, C.; Hodgeman, D.; Chater, P. A.; Demont, A.; Romani, S.; Sayers, R.; Thomas, M. F.; Claridge, J. B.; Darling, G. R.; Rosseinsky, M. J. Computationally assisted identification of functional inorganic materials. *Science* **2013**, *340*, 847–852.
- (46) Kang, L.; Luo, S.; Peng, G.; Ye, N.; Wu, Y.; Chen, C.; Lin, Z. First-Principles Design of a Deep-Ultraviolet Nonlinear-Optical Crystal from KBe₂BO₃F₂ to NH₄Be₂BO₃F₂. *Inorg. Chem.* **2015**, 54, 10533–10535.
- (47) Lei, B.-H.; Yang, Z.; Yu, H.; Cao, C.; Li, Z.; Hu, C.; Poeppelmeier, K. R.; Pan, S. Module-Guided Design Scheme for Deep-Ultraviolet Nonlinear Optical Materials. *J. Am. Chem. Soc.* **2018**, 140, 10726–10733.
- (48) Lin, Z.; Jiang, X.; Kang, L.; Gong, P.; Luo, S.; Lee, M.-H. First-principles materials applications and design of nonlinear optical crystals. *J. Phys. D: Appl. Phys.* **2014**, *47*, 253001.

- (49) Ok, K. M.; Halasyamani, P. S.; Casanova, D.; Llunell, M.; Alemany, P.; Alvarez, S. Distortions in Octahedrally Coordinated d0Transition Metal Oxides: A Continuous Symmetry Measures Approach. *Chem. Mater.* **2006**, *18*, 3176–3183.
- (50) Yang, Z.; Lei, B.-H.; Zhang, W.; Pan, S. Module-Analysis-Assisted Design of Deep Ultraviolet Fluorooxoborates with Extremely Large Gap and High Structural Stability. *Chem. Mater.* **2019**, *31*, 2807–2813.
- (51) Chen, X.; Zhang, B.; Zhang, F.; Wang, Y.; Zhang, M.; Yang, Z.; Poeppelmeier, K. R.; Pan, S. Designing an Excellent Deep-Ultraviolet Birefringent Material for Light Polarization. *J. Am. Chem. Soc.* **2018**, 140, 16311–16319.
- (52) Wu, H.; Yu, H.; Yang, Z.; Hou, X.; Su, X.; Pan, S.; Poeppelmeier, K. R.; Rondinelli, J. M. Designing a deep-ultraviolet nonlinear optical material with a large second harmonic generation response. *J. Am. Chem. Soc.* **2013**, *135*, 4215–4218.
- (53) Zhang, B.; Shi, G.; Yang, Z.; Zhang, F.; Pan, S. Fluorooxoborates: Beryllium-Free Deep-Ultraviolet Nonlinear Optical Materials without Layered Growth. *Angew. Chem., Int. Ed. Engl.* **2017**, *56*, 3916–3919.
- (54) Bian, Q.; Yang, Z.; Dong, L.; Pan, S.; Zhang, H.; Wu, H.; Yu, H.; Zhao, W.; Jing, Q. First Principle Assisted Prediction of the Birefringence Values of Functional Inorganic Borate Materials. *J. Phys. Chem. C* 2014, *118*, 25651–25657.
- (55) Aoyagi, S.; Kuroiwa, Y.; Sawada, A.; Yamashita, I.; Atake, T. Composite Structure of BaTiO₃ Nanoparticle Investigated by SR X-Ray Diffraction. *J. Phys. Soc. Jpn.* **2002**, *71*, 1218–1221.
- (56) Bernuy-Lopez, C.; Allix, M.; Bridges, C. A.; Claridge, J. B.; Rosseinsky, M. J. Sr₂MgMoO₆-δ: Structure, Phase Stability, and Cation Site Order Control of Reduction. *Chem. Mater.* **2007**, *19*, 1035–1043.
- (57) Sutton, R. J.; Filip, M. R.; Haghighirad, A. A.; Sakai, N.; Wenger, B.; Giustino, F.; Snaith, H. J. Cubic or Orthorhombic? Revealing the Crystal Structure of Metastable Black-Phase CsPbI₃ by Theory and Experiment. *ACS Energy Lett.* **2018**, *3*, 1787–1794.
- (58) Weller, M. T.; Weber, O. J.; Henry, P. F.; Di Pumpo, A. M.; Hansen, T. C. Complete structure and cation orientation in the perovskite photovoltaic methylammonium lead iodide between 100 and 352 K. Chem. Commun. 2015, 51, 4180–4183.
- (59) Sabrowsky, H.; Feldbaum-Möller, E.; Fischer, K.; Sitta, S.; Vogt, P.; Winter, V. Die Kristallstrukturen von α und β -K₃OCl. Z. Anorg. Allg. Chem. **1996**, 622, 153–156.
- (60) Lei, B.-H.; Yang, Z.; Pan, S. Enhancing optical anisotropy of crystals by optimizing bonding electron distribution in anionic groups. *Chem. Commun.* **2017**, *53*, 2818–2821.
- (61) Lin, J.; Lee, M.-H.; Liu, Z.-P.; Chen, C.; Pickard, C. J. Mechanism for linear and nonlinear optical effects in β -BaB₂O₄ crystals. *Phys. Rev. B: Condens. Matter Mater. Phys.* **1999**, 60, 13380–13389.
- (62) Perdew, J. P.; Levy, M. Physical Content of the Exact Kohn-Sham Orbital Energies: Band Gaps and Derivative Discontinuities. *Phys. Rev. Lett.* **1983**, *51*, 1884–1887.
- (63) Aversa, C.; Sipe, J. E. Nonlinear optical susceptibilities of semiconductors: Results with a length-gauge analysis. *Phys. Rev. B: Condens. Matter Mater. Phys.* **1995**, *52*, 14636–14645.
- (64) Xia, Z.; Poeppelmeier, K. R. Chemistry-Inspired Adaptable Framework Structures. Acc. Chem. Res. 2017, 50, 1222–1230.
- (65) Clark, S. J.; Segall, M. D.; Pickard, C. J.; Hasnip, P. J.; Probert, M. J.; Refson, K.; Payne, M. C. First principles methods using CASTEP. Z. Kristallogr. 2005, 220, 567–570.
- (66) Perdew, J. P.; Burke, K.; Ernzerhof, M. Generalized Gradient Approximation Made Simple. *Phys. Rev. Lett.* **1996**, *77*, 3865–3868.
- (67) Monkhorst, H. J.; Pack, J. D. Special points for Brillouin-zone integrations. *Phys. Rev. B: Solid State* 1976, 13, 5188–5192.
- (68) Levine, Z. H.; Allan, D. C. Quasiparticle calculation of the dielectric response of silicon and germanium. *Phys. Rev. B: Condens. Matter Mater. Phys.* **1991**, 43, 4187–4207.

The Journal of Physical Chemistry C

- (69) Wemple, S. H. Polarization Fluctuations and the Optical-Absorption Edge in BaTiO₃. *Phys. Rev. B: Solid State* **1970**, *2*, 2679–2689
- (70) Kim, D. H.; Kwok, H. S. Pulsed laser deposition of BaTiO₃ thin films and their optical properties. *Appl. Phys. Lett.* **1995**, *67*, 1803–1805
- (71) Wu, H.; Yu, H.; Yang, Z.; Han, J.; Wu, K.; Pan, S. Linear optical and thermo-physical properties of polar $K_3B_6O_{10}Cl$ crystal. *J. Materiomics* **2015**, *1*, 221–228.
- (72) Jia, W.; Cao, Z.; Wang, L.; Fu, J.; Chi, X.; Gao, W.; Wang, L.-W. The analysis of a plane wave pseudopotential density functional theory code on a GPU machine. *Comput. Phys. Commun.* **2013**, *184*, 9–18.